

From compact to fractal crystalline clusters in concentrated systems of monodisperse hard spheres

Chantal Valeriani,^{1,2} Eduardo Sanz,^{1,2} Peter N. Pusey,² Wilson C. K. Poon,² Michael E. Cates,² and Emanuela Zaccarelli³

¹*Departamento de Química Física, facultad de Ciencias Químicas, Universidad Complutense, 28040 Madrid, Spain*

²*SUPA, School of Physics and Astronomy, University of Edinburgh, Mayfield Road, Edinburgh, EH9 3JZ, Scotland*

³*CNR-ISC and Dipartimento di Fisica, Università di Roma La Sapienza, P.le A. Moro 2, 00185 Roma, Italy*

We address the crystallization of monodisperse hard spheres in terms of the properties of finite-size crystalline clusters. By means of large scale event-driven Molecular Dynamics simulations, we study systems at different packing fractions ϕ ranging from weakly supersaturated state points to glassy ones, covering different nucleation regimes. We find that such regimes also result in different properties of the crystalline clusters: compact clusters are formed in the classical-nucleation-theory regime ($\phi \leq 0.54$), while a crossover to fractal, ramified clusters is encountered upon increasing packing fraction ($\phi \geq 0.56$), where nucleation is more spinodal-like. We draw an analogy between macroscopic crystallization of our clusters and percolation of attractive systems to provide ideas on how the packing fraction influences the final structure of the macroscopic crystals. In our previous work (*Phys. Rev. Lett.*, **106**, 215701, 2011), we have demonstrated how crystallization from a glass (at $\phi > 0.58$) happens via a gradual (many-step) mechanism: in this paper we show how the mechanism of gradual growth seems to hold also in super-saturated systems just above freezing showing that static properties of clusters are not much affected by dynamics.

I. INTRODUCTION

Following the pioneering computer simulations of Alder and Wainwright [1], more than 50 years ago, assemblies of hard spheres in thermal motion have become the subject of intense research aimed at unveiling the fundamental physics of both thermodynamic and kinetic phase transitions. This numerical work has been complemented by experimental studies of suspensions of “hard-sphere” colloidal particles (see Ref. [2–5]).

Despite the simplicity of the hard-core interactions, the behaviour of this system is far from trivial and several important questions still remain unanswered. Concerning thermodynamics, the location of the fluid-to-crystal transition, occurring in the packing fraction ϕ range $0.492 < \phi < 0.543$ has been quite well characterised [1, 6–8]. However, open issues remain concerning the effect of polydispersity [9–11] and, most importantly, the reported discrepancy between calculated nucleation rates and those measured experimentally [12]. These issues have recently caused a revival of studies on hard-sphere nucleation [13–16]. In particular, recent works aim to elucidate the mechanism of crystal formation in terms of preferred precursor structures [17–19], proposing a two-step scenario [20, 21], and also aim to assess the competition between different solid polymorphs [22].

Not only does the fluid-to-crystal transition remain debated, but also the presence of an ideal glass transition at packing fractions below random close packing ($\phi_{rcp} \approx 0.64$) is still under discussion. The initial observations by Pusey and van Meegen [2] of a glass transition taking place for $\phi \sim 0.58$ were later challenged by works in microgravity [23, 24] and by numerical simulations by Torquato and coworkers [25]. Moreover, a recent work by Brambilla et al. [26] caused considerable debate in

the glass community [27–29]. By considerably extending the observation time window, these authors suggested that the glass transition was always obviated by activated processes whenever $\phi < \phi_{rcp}$. However, delicate issues remain, concerning for example the correct way of estimating the “true” colloidal packing fraction in these experiments [30].

With this as background, we have recently started an extensive numerical investigation of hard-sphere systems, via event-driven Molecular Dynamics simulations. Initially, we assessed the role of polydispersity on dynamics and crystallization [13, 31], finding that, while changing substantially the nucleation behaviour, a small degree of polydispersity $s \lesssim 6\%$ does not strongly affect the dynamics, leaving unchanged the tendency to form an ideal glass around 0.58 [31]. In addition, we identified two regimes of nucleation [13, 32]: standard nucleation and growth at concentrations in and slightly above the coexistence region and, beyond $\phi \sim 0.56$, “spinodal nucleation”, where the free energy barrier to nucleation appears to be negligible. In the latter regime, at very high volume fractions, we have investigated the subtle interplay between slow dynamics and crystallization, elucidating a novel mechanism by which hard-sphere glasses crystallize without particle diffusion (even at the single particle level) on scales comparable to or beyond their radius [33]. Diffusionless crystallisation has also been recently reported for a 3 dimensional lattice system [34].

In this work, we investigate an aspect of crystallisation of monodisperse hard spheres that, to our knowledge, has not been studied so far: the statistics properties of crystalline clusters as crystallisation proceeds. By monitoring a large system, we identify the solid-like clusters and analyse their size distribution and shape as a function of packing fraction and of time. These clusters undergo a percolation transition of the kind described

in simulation [35] and in theoretical work on molecular systems [36]. We monitor the cluster size distribution and clusters radius of gyration as a function of time, to address whether non-trivial exponents can be extracted and related to the standard percolation scenario that is commonly encountered in attractive systems [37].

A comment is due on the definition of clusters of hard-sphere particles, where no attraction is present. Indeed, clusters are rigorously defined [38] for attractive systems in terms of an energy scale which cohesively keep particles together. Moreover, in the case of colloidal particles interacting with competing short-ranged attraction (e.g. depletion) and long-ranged repulsion (induced by electrostatics), clusters are found to be stable minima of the underlying potential [39–42]. These equilibrium clusters have been observed in both experiments and simulations [43–46] and their role as a building blocks of non-equilibrium structures like Wigner glasses and gels is still under active investigation [40, 47–52]. In the case of hard spheres, particles forming a cluster “glue” due to the thermodynamic driving force toward crystal nucleation [53, 54] rather than due to attractive interactions between particles. Hence, whenever we find two nearest-neighbour solid-like particles (according to the definitions discussed below), we consider them as belonging to the same crystalline cluster. Of course, these clusters can be either transient or permanent, in analogy with attractive clusters at finite temperature.

Within our study, we cannot monitor the equilibrium distribution of such clusters because of the irreversible process of crystallization once it is triggered. However, we can follow their growth while crystallization proceeds, so that with time clusters become larger and larger and consequently more and more permanent, until macroscopic crystallization of the samples occur. In particular, we study crystallization at different packing fractions, in order to address the question of whether significant differences can be found between the different nucleation regimes. Our findings suggest an important crossover from compact to fractal clusters with increasing supersaturation, which reflects the change in the underlying crystallisation processes. These findings could have important consequences for the final structures of the resulting macroscopic crystals.

The manuscript is organised as follows: we first present the simulation and analysis method in Section II; next, we report our results on the clusters structure at different packing fractions (Section III A), the percolation of the crystalline clusters (Section III B), the cluster size distribution (Section III C) and on the effect of the criterion to identify solid-like particle on properties of the growing crystalline clusters (Section III D).

II. SIMULATION AND ANALYSIS METHODS

We perform event-driven Molecular Dynamics simulations in the NVT ensemble with cubic periodic boundary

conditions for a large system of $N = 86400$ monodisperse hard spheres [55, 56]. Mass, length, and time are measured in units of particle mass m , particle diameter σ and $\sqrt{m\sigma^2/\kappa_B T}$, where κ_B is the Boltzmann constant and T the temperature and we set $\kappa_B T = 1$. The system is prepared at different packing fractions $\phi = \frac{\pi}{6} N \sigma^3 / V$ (with V the system’s volume) beyond freezing ranging from $\phi = 0.54$ to $\phi = 0.61$. At $\phi \geq 0.54$, the metastable fluid-phase spontaneously crystallizes within the duration of our simulations. With increasing ϕ , the relaxation of the system becomes slower and slower, until the glass transition around $\phi \sim 0.58$ is encountered [31]. Above this value, ageing effects are present and crystallization occurs from a glass [33].

To study the formation and growth of crystalline clusters, we first identify the solid particles in the system. To this end, we use the rotationally invariant local bond order parameter d_6 defined as the scalar product between particle i ’s q_6 complex vector and the one of each of its neighbour j , $d_6(i, j)$ (see Appendix A for further details). Once we have identified all solid particles N_s in the system, we monitor the fraction of crystalline particles, defined as $X = \frac{N_s}{N}$. To identify crystalline clusters, we run a cluster-algorithm: starting from a solid particle, we locate its solid neighbours within a distance of 1.4σ and define them as belonging to the same cluster. After having iteratively applied the cluster-algorithm to all solid particles in the system, at every time-step we identify all crystalline clusters and compute their size (s).

To improve the statistics of our results, we consider 10 independent crystallisation trajectories for each studied packing fraction, each initiated from configurations without pre-existing crystal nuclei. In order to achieve this non-trivial condition, we compress a small system of 400 particles to a high packing fraction, $\phi = 0.64$, monitoring that the fraction of crystalline particles is less than 0.005 of the total number of particles. We then replicate this system periodically in space, checking that any sign of periodicity resulting from the replication procedure is lost after a very short time (as in Ref. [33]). Next, before starting Molecular Dynamics runs, we isotropically expand the configuration to the desired packing fraction.

First of all, we perform an analysis of the structure of the growing crystalline clusters at different packing fractions. This is done both qualitatively, monitoring the structure of the clusters that are visible in the snapshots taken from our simulations and quantitatively, studying the size-dependence of the cluster’s radius of gyration:

$$R_g = \left[\frac{1}{s} \sum_{i=1}^s \left| \vec{r}_i - \vec{R}_{CM} \right|^2 \right]^{1/2} \quad (1)$$

where s is the number of particles in the cluster (i.e. the cluster size), \vec{r}_i indicates the position of particle i and \vec{R}_{CM} is the position of the centre of mass of the cluster. For fractal aggregates, the dependence of the radius of gyration on the cluster size follows a power law, i.e. $R_g \sim s^{1/d_f}$, where d_f is the fractal dimen-

sion of the aggregation process. For random percolation in three dimensions, the value of d_f is known to be about 2.5 [37]. For spherical clusters $R_g \sim s^{1/3}$, whereas for planar (loose) clusters $R_g \sim s^{1/2}$ and for linear ones $R_g \sim s$ [37, 45].

Next, we study the percolation of crystalline clusters by estimating the first time when a system-spanning cluster appears in the simulation box, i.e., the percolation time τ_p . In practice, we detect τ_p as the time when the largest crystalline cluster becomes infinite according to our periodic boundary conditions criterion. After having identified, at each time-step, the largest crystalline cluster, we replicate the simulation box and check whether we get a single cluster in the replicated system: the time when this happens defines τ_p (which is then averaged over independent runs). Once τ_p is known, we estimate the value of the total crystallinity at percolation $X(\tau_p) = X_p$. Even though we are aware that an accurate location of the percolation threshold would require a finite-size scaling analysis, our aim is not to define with high precision the percolation threshold, but rather to find a link between the percolation transition and macroscopic crystallization.

We also calculate the cluster size distribution, i.e. the fraction of clusters with s solid-like particles. The cluster size distribution changes with time during the crystallization process. To reduce its numerical noise, we evaluate it for configurations of independent trajectories having approximately the same crystallinity, using narrow X intervals of width $\Delta X = 0.01$. In this way we can average our results over all trajectories within a given X -interval and over the 10 independent runs. According to random percolation theory, the cluster size distribution in a three dimensional system decays exponentially fast for large s below the percolation threshold, whereas it follows a power-law behaviour at percolation, i.e. $s^{-\tau}$ (where $\tau \simeq 2.2$ [37]).

Finally, to assess the role of the particular choice of parameters used to define solid-like clusters, we analyse the effect of the “solid-like” criterion on the clusters radius of gyration, considering different choices of the number of solid-like connections ξ_c needed to identify a solid-like particle.

III. RESULTS

We present our results as follows: in Section III A we perform both a qualitative and a quantitative analysis of the clusters’ structure for packing fractions ranging from $\phi = 0.54$ to $\phi = 0.61$; in Section III B we study percolation of the crystalline clusters; in Section III C we estimate the cluster size distribution. In the last Section, III D, we analyse the effect of the criterion used to identify solid-like particle on properties of the growing crystalline clusters.

A. Structure of the growing crystalline clusters

First, we study the characteristic structure of growing crystallites at different packing fractions ϕ . In order to visualise how the structure of crystalline clusters changes with increasing packing fraction, we follow the largest cluster during the simulation run, as represented in Figure 1. When $\phi = 0.54$ (left-most panel in Figure 1), we observe a rather homogeneous and compact cluster, whereas more ramified structures emerge at higher ϕ (e.g. $\phi = 0.56, 0.58, 0.61$). An intermediate case is $\phi = 0.55$ (second panel from the left in Figure 1) clearly showing small compact clusters connected to each other via thin branches.

As we have already discussed elsewhere [13, 33], there is a strong correlation between the crystallization mechanism and the packing fraction of the system. For $\phi = 0.54$, crystallization appears to follow the classical nucleation theory (CNT) picture where a critical cluster needs to form in order for crystallization to proceed. Once a crystalline cluster overcomes a critical size, it grows in an almost compact structure and the entire system crystallizes (“classical nucleation and growth” regime). Having used a large system and being at a relatively high supersaturation (with respect to freezing), we detect more than one critical cluster in the system (of the order of 2-3): all these clusters are compact, can form anywhere in the system, grow independently and, eventually, merge together. When $\phi \geq 0.56$ (“spinodal-like crystallization” regime), a random crystal growth habit is reached, where crystallization takes place everywhere in the system. The free-energy barrier of nucleation gets closer to zero the higher the packing fraction, and no critical cluster size needs to be exceeded in order for crystallization to proceed. Crystallization proceeds via branching of ramified clusters as X grows (right-most snapshot in Figure 1) and this mechanism is reminiscent of a percolation transition associated with the crystallization process: moreover, at $\phi > 0.58$, crystallization happens without particles diffusing more than a diameter [33]. As said above, the case at $\phi = 0.55$, where branching connections of more compact (and finite) clusters are found, is intermediate between $\phi = 0.54$ and higher packing fractions ($\phi > 0.56$).

To quantify the structure of the crystalline clusters, we measure their radius of gyration (R_g) as a function of their sizes at all packing fractions and extract from it an effective fractal dimension d_f , via $R_g \sim s^{1/d_f}$ (see Figure 2). To improve the statistics, data are averaged over all equal-sized clusters, over 10 trajectories and over time.

In Figure 2 we observe that, at all packing fractions, the radius of gyration for small clusters follows $R_g \sim s^{1/2}$. When clusters become larger ($s > 50$), their fractal dimension starts to be larger than 2 and their internal structure changes depending on ϕ . Two distinct behaviours emerge: one pertaining to $\phi = 0.54$ and another to $\phi \geq 0.56$ (as shown by the superposition of the data in Figure 2). When $\phi = 0.54$, crystallization fol-

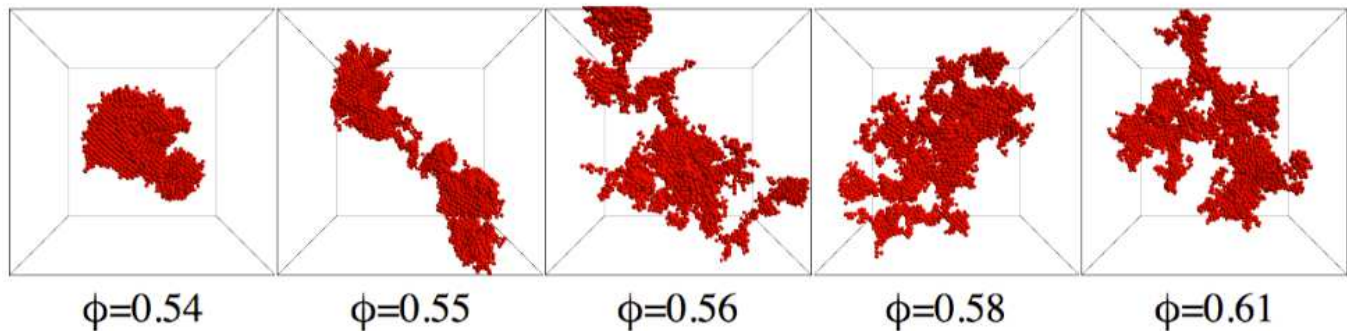


FIG. 1: Snapshots of typical largest crystalline clusters as a function of ϕ at fixed cluster size ($s = 5000$). This size is achieved when (ϕ, X) are respectively $(0.54, 0.08)$, $(0.55, 0.15)$, $(0.56, 0.15)$, $(0.58, 0.14)$, $(0.61, 0.12)$. Periodic boundary conditions are taken into account and clusters are centred in the simulation box.

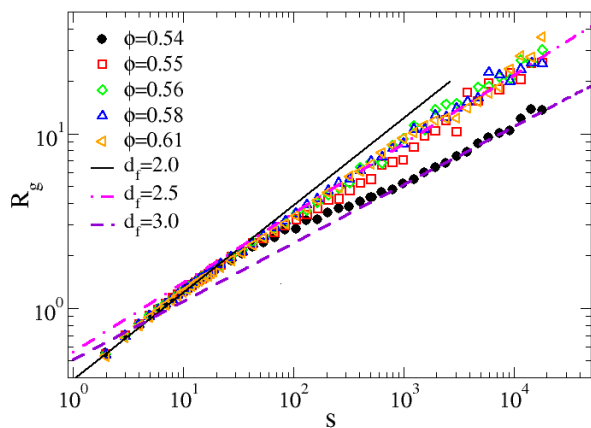


FIG. 2: Radius of gyration (R_g) versus clusters-size (s) at various ϕ (s is averaged over different runs and over time). As a guide to the eye, we plot $R_g \sim s^{1/d_f}$, with $d_f = 2.0$ (continuous black curve), 2.5 (dashed magenta curve) and 3.0 (dashed blue curve).

lows the standard CNT picture, i.e. the system has to overcome a free-energy barrier in order to transform into a crystal. Hence, nucleation is a rare event and clusters appear and disappear in a stochastic way until the critical size is reached. The critical cluster size at this ϕ is estimated with CNT to be of the order of $s_c \sim 50$ [13]. As it can be observed from Figure 2, beyond this critical value clusters show a marked change in their fractal dimension, becoming more and more compact (value of d_f increasing). When the cluster size exceeds ≈ 300 , the data clearly follow the exponent $d_f = 3$, characteristic of a compact cluster (such as the corresponding cluster in Figure 1) [58]. Hence, we conclude that, at this ϕ (and in the CNT-regime), the structure of the clusters is mainly determined by their size.

When $\phi \geq 0.56$, nucleation is not an activated pro-

cess any more (there is no free-energy barrier to overcome [13]) and all R_g data scale onto the same master curve: after a loose/open growth of the small clusters, as soon as $s > 50$, clusters grow following the scaling predicted for random percolation in 3D with fractal dimension $d_f \sim 2.5$. This is consistent with the snapshots presented in Figure 1, where already at $\phi = 0.56$ clusters start to be ramified and crystallization occurs with the growth of clusters appearing almost everywhere in the system. However, as we will discuss in Section III C, clusters do not grow completely at random; instead they tend to form in the vicinity of already existing ones [33]. This is even more evident at packing fractions beyond $\phi = 0.58$, due to particles' lack of diffusion on the scale of their radius.

Finally we discuss the case $\phi = 0.55$, where we observe signatures of an intermediate behaviour. Given that the nucleation free-energy barrier is quite low, clusters start growing everywhere in the system, create a branch-like structure when they grow larger (as shown in the snapshot of Figure 1), and R_g shows an intermediate behaviour between the compact scaling of the CNT regime and the fractal one pertaining to the spinodal-like regime (as shown in Figure 2).

B. Percolation analysis

We now perform an analysis of the percolation of the largest crystalline cluster in the system for all studied packing fractions, identifying both the percolation time τ_p and the value of the crystallinity at percolation X_p .

In Figure 3 we report the dependence of X_p on ϕ and observe that, for increasing values of ϕ , the crystallinity at the percolation transition has a monotonically decreasing behaviour, that is steeper for $\phi < 0.56$ than for $\phi \geq 0.56$. To interpret this result we recall our previous findings that clusters are more compact with decreasing ϕ for $\phi < 0.56$. Hence, in order to percolate, the largest cluster needs to reach a larger size than the one needed at higher ϕ . On the other hand, when $\phi \geq 0.56$ d_f re-

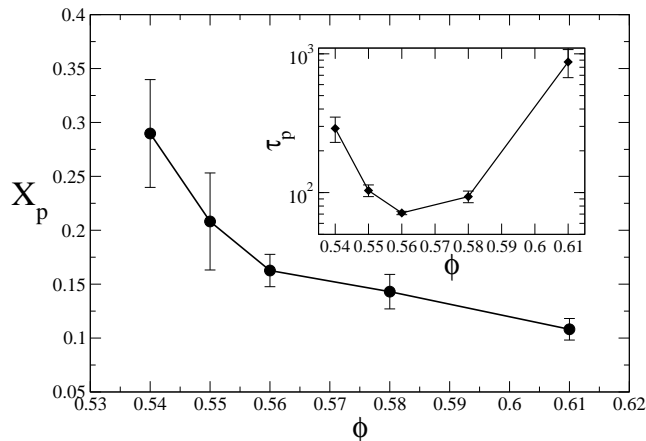


FIG. 3: Fraction of crystalline particles at the percolation threshold X_p as a function of ϕ . Inset: percolation time τ_p as a function of ϕ .

mains constant so that X_p does not change much with ϕ . Due to the stochastic nature of nucleation at $\phi = 0.54$, that results in a small number of growing clusters that is different for each independent run, the X_p error bar is larger at the lowest packing fractions.

For $\phi \geq 0.56$ crystalline clusters are found to percolate when the total crystallinity of the system is $X_p \approx 0.10$ – 0.15 . The fact that the overall crystallization needs to be at least 0.1 in order to observe percolation of the crystalline clusters (made of purely repulsive spheres) has an analog in studies of percolation of attractive clusters (made of particles interacting via short-range attraction and screened electrostatic repulsion) [45]. In fact, it has been shown that in such systems, when the colloidal packing fraction ϕ_c is about 0.10, attractive clusters (whose size distribution obeys a power law with an exponent typical of random percolation) percolate throughout the system.

So far, we have presented only *static* observations of the structure of the growing clusters. In the inset of Figure 3 we plot *kinetic* results of the clusters growth, representing the percolation time τ_p as a function of ϕ . Contrary to the monotonic decrease of X_p , τ_p displays a clear minimum at intermediate ϕ . The fastest percolation of the largest cluster is at $\phi = 0.56$ when the largest cluster is already branched but particles can still easily diffuse. Whereas at low ϕ the percolation time is longer due to the compact structure of the growing cluster (requiring a larger X_p), at large ϕ percolation slows down due to the slowing of particles dynamics. This behaviour is remarkably similar to that observed for the “nucleation time” $\tau_n(\phi)$, defined as time at which $X = 0.2$, that corresponds to the time when the system is strongly committed to crystallize [13]: at low ϕ , nucleation is slow (large τ_n) due to a high nucleation free-energy barrier, while at large ϕ nucleation slows down again due to the slowing particle dynamics; the fastest nucleation (smallest τ_n) occurs around $\phi = 0.56$, where the free-energy barrier is

very low and diffusion still possible. Therefore, the percolation of the growing clusters is correlated to the commitment of the system to fully crystallize. We stress that at large ϕ , despite the slowing down of particles dynamics, percolation is achieved with lower crystallinity than at lower ϕ . Hence, the kinetic slowing down is probably responsible for the continuous decrease of X_p , even when the shape of the clusters (quantified by d_f) stops changing. Indeed, we find that $X_p(\phi = 0.61)$ is almost a factor of 3 smaller than $X_p(\phi = 0.54)$, whereas $\tau_p(\phi = 0.61)$ is around 3 times larger than $\tau_p(\phi = 0.54)$, due to the slowing down of the dynamics beyond the glass transition (occurring at $\phi \sim 0.58$ [2, 31]).

The behaviour of X_p with ϕ can also be rationalised by looking at the total number of clusters N_c . In the inset of Figure 4, we report N_c as a function of X for different packing fractions.

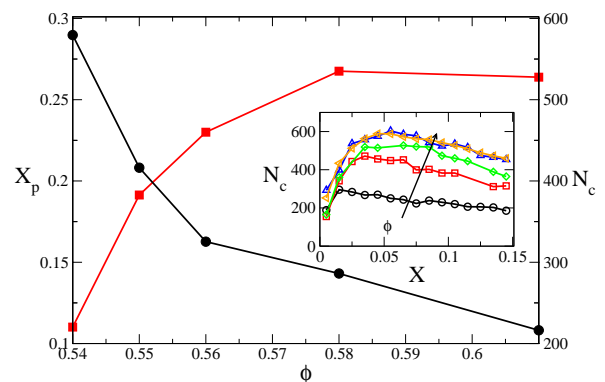


FIG. 4: X_p (black curve) and $N_c(X = 0.10)$ (red curve) as a function of ϕ . Inset: N_c as a function of X (averaged within a $\Delta X = 0.01$ interval and over independent trajectories) at different ϕ (from bottom to top curve: $\phi = 0.54, 0.55, 0.56, 0.58, 0.61$).

It is evident that, for a given X , the number of clusters increases with increasing ϕ , due to the reduced free-energy barrier, and it saturates when $\phi \geq 0.58$. In particular, for $\phi = 0.54$, the maximum number of clusters occurs at very small values of X , where one or more critical nuclei have already formed and grow by single particles or small clusters attaching to them (that explains the slow decrease of N_c with increasing X). On the other hand, with increasing ϕ , N_c keeps increasing for small values of X (since many small clusters can easily form) until it starts decreasing from $X \sim 0.03$ – 0.05 (where clusters start to branch). We also observe a clear dependence on ϕ below the glass transition ($\phi = 0.58$). This can be better seen by looking at N_c for a fixed value of X , e.g. $X = 0.10$, which is reported in Figure 4 together with X_p as a function of ϕ . Comparing the behaviour of N_c to X_p , we can rationalise the decrease of the latter as being related to the increase of the total number of clusters up to $\phi \sim 0.58$. For larger ϕ , N_c remains constant and the decrease of X_p could be partially ascribed to the increase of packing fraction, so that even if the number

of the clusters is the same, the number of clusters per unit volume is higher and percolation happens at lower X . Moreover, minor differences within the statistical error of our analysis of the clusters shape and the cluster size distribution (see next Section) could also contribute to the decrease of X_p from $\phi = 0.58$ to $\phi = 0.61$.

C. Cluster size distribution

In this section we discuss the behaviour of the cluster size distribution. $n(s)$ represents the number of clusters of size s and $f(s)$ the fraction of such clusters, i.e. $n(s)$ divided by the total number of clusters N_c . $n(s)$ varies as crystallization proceeds. To improve the statistics, we average over 10 independent trajectories and within X intervals of width 0.01. For all packing fractions we calculate $n(s)$ and $f(s)$ for crystallinity up to $X = 0.15$; at this value, crystalline clusters have not percolated yet at $\phi = 0.54$ and $\phi = 0.55$ (Figure 3) and have just percolated (on average) for $\phi \geq 0.56$. However, in the analysis that follows we have excluded percolating clusters.

In Figure 5 we report $n(s)$ for different X -intervals both for $\phi = 0.54$ (top) and $\phi = 0.61$ (bottom). For both packing fractions, $n(s)$ shows a rapid decay for $X < 0.01$ signaling the growth of the first few crystalline clusters. Once $X \geq 0.03$ (when $\phi = 0.54$) and $X \geq 0.06$ (when $\phi = 0.61$), all curves collapse onto each other, showing that the clusters distribution has reached a stationary profile during crystal growth. This happens for all studied ϕ and justifies further averaging of the $n(s)$ curves over all configurations within the range $0.06 < X < 0.14$ [59]. We also notice that large clusters, e.g. $s \gtrsim 100$, are rare in the case of $\phi = 0.54$ while their number becomes very large for $\phi = 0.61$, as indicated respectively by scarce/abundant population of large- s points in Figure. 5.

We now focus on the fraction of clusters of size s , $f(s)$. In order to evaluate $f(s)$ for increasingly large s (where clusters of each size become more and more scarce), we apply the following criterion: (i) we arbitrarily subdivide the range of s -values into intervals $\Delta s_i = (s_{i,max} - s_{i,min})$ containing at least one cluster each and estimate n_i^t , i.e. the total number of clusters within each interval Δs_i ; (ii) we assign the value of $n_i = n_i^t / \Delta s_i$ to every s within Δs_i . The total number of clusters can be computed as $N_c = \sum_i n_i \Delta s_i$ and the fraction of clusters of size s , $f(s) = n_i / N_c$. We now represent $f(s)$ as a function of s , the closest integer to the central value of Δs_i . We leave to the Appendix B the definition of all $\Delta s_i = (s_{i,max} - s_{i,min})$ intervals. In Figure 6 we plot $f(s)$ for several packing fractions ranging from 0.54 to 0.61. Data are averaged for $0.06 < X < 0.14$ (within this range we have found the profiles to be stationary and independent of X [59]).

First of all, we notice the marked difference that is found between the data corresponding to $\phi = 0.54$ and all other data. This demonstrates that the stationary

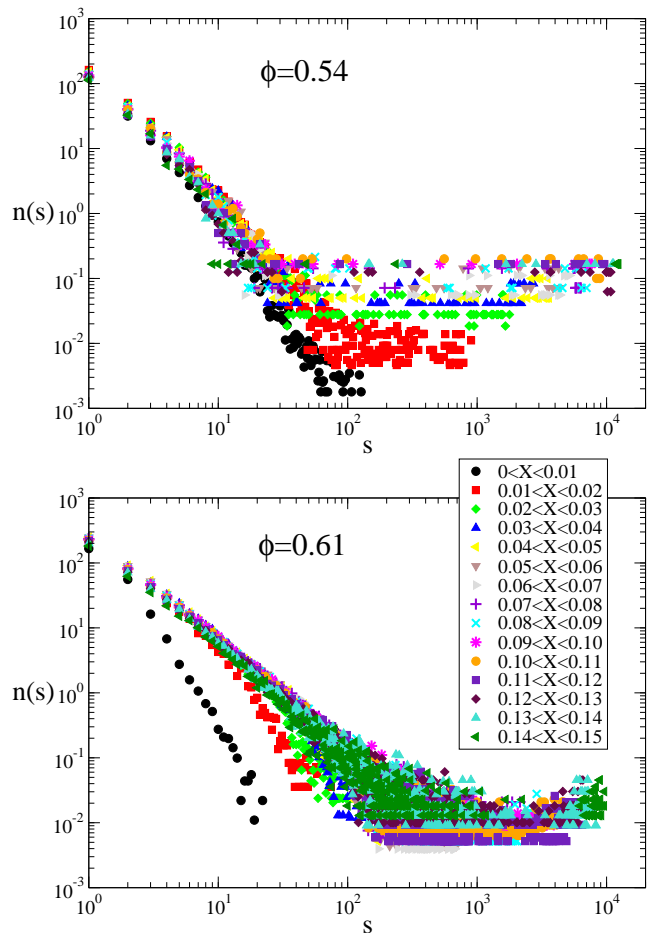


FIG. 5: Number of clusters $n(s)$ at $\phi = 0.54$ (top) and $\phi = 0.61$ (bottom). Each data set is averaged over 10 independent runs in intervals ranging from $0.0 \leq X \leq 0.01$ to $0.14 \leq X \leq 0.15$ ($\Delta X = 0.01$). $n(s)$ can take values smaller than 1, being computed as the number of clusters for each value of s divided by the number of runs and by the number of configurations analysed for a given X window. Symbols are the same for both panels. Only non-percolating clusters are considered in the analysis.

cluster size distribution is, within our statistical uncertainty, identical for any ϕ larger than 0.55. This behaviour is similar to what we observed for R_g , pointing to the universality of (static) properties of the clusters once spinodal-like nucleation has occurred.

From the calculated $f(s)$ we can search for the emergence of a power-law behaviour approaching crystallization, in analogy with standard attractive systems approaching a percolation transition. We find that when $\phi = 0.54$ a crossover between two regimes takes place at $s^* = 50$, which corresponds to the estimate of the critical cluster size according to CNT [13]. For $s < s^*$ the cluster distribution is not too different from that of a system approaching random percolation ($f(s) \sim s^{-2.2}$); whereas larger clusters grow in a compact way, resulting in a much lower power-law exponent ($f(s) \sim s^{-1.0}$). When $\phi \geq 0.55$, $f(s)$ seems to follow a power law with

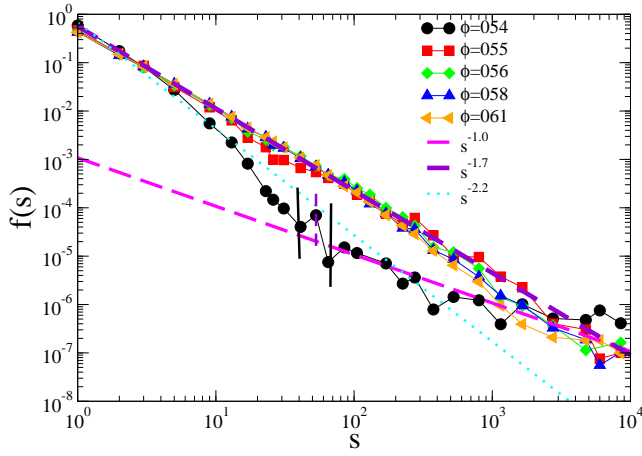


FIG. 6: Fraction of clusters of size s , $f(s)$, averaged over the X -intervals where the curves collapse ($0.06 < X \leq 0.14$ at all ϕ). As a guide to the eye, we also plot the power-law dependence of $s^{-1.0}$ (dashed magenta curve), $s^{-1.7}$ (dashed violet curve) and $s^{-2.2}$ (dotted cyan curve). Only non-percolating clusters are considered in the analysis. The vertical lines $s^* = 50 \pm 10$ indicates the crossover between two regimes at $\phi = 0.54$.

exponent $\tau \sim 1.7$ for the entire size range (even for very small cluster sizes). We notice that this value for τ is similar to that of the exponent found for the size distribution of mobile regions in glass-forming systems [60]. The discrepancy with the exponent expected from random percolation theory ($\tau \sim 2.2$) may stem from the fact that new crystalline regions preferably appear in the surroundings of existing ones [33], which causes a partial loss of randomness of the growing aggregate.

We now analyse further the behaviour of $f(s)$ for $\phi = 0.54$ by using CNT, where a clear crossover between two regimes is present. When s is small, sub-critical clusters form and re-dissolve whereas when s is large post-critical clusters irreversibly grow. Only the large- s regime seems to follow convincingly a power law with exponent $\tau \sim 1$, whereas the small- s regime starts deviating from random aggregation ($\tau \sim 2.2$) when s approaches s^* . According to CNT [53], the free-energy barrier associated to the appearance of size- s clusters is written as $\beta\Delta G(s) = -\ln(P(s))$, where $P(s) = n(s)/N$ is the probability to have size- s clusters in the system. Therefore, we can use the cluster size distribution $n(s)/N$ (or equivalently $f(s) \times N_c/N$) to estimate the barrier, as shown in Figure 7 for different packing fractions (averaged over the range $0.06 < X < 0.14$).

At all packing fractions higher than 0.55 the curves in Figure 7 collapse, showing that crystallites starts growing in the same way whenever $\phi > 0.55$: multiple crystalline patches appear and crystallization proceeds by a sequence of stochastic micronucleation events, correlated in space by emergent dynamic heterogeneity [33]. As we have already mentioned, the case when $\phi = 0.55$ is intermediate between $\phi > 0.55$ and $\phi = 0.54$. When

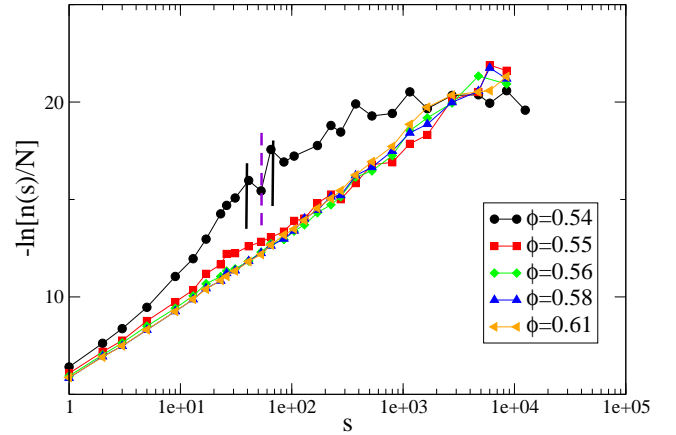


FIG. 7: $-\ln(n(s)/N)$ versus s for $0.54 \leq \phi \leq 0.61$. $n(s)/N = f(s) \times N_c/N$ (where $f(s)$ data are from Figure 6). The vertical lines $s^* = 50 \pm 10$ indicates the crossover between two regimes at $\phi = 0.54$.

$\phi = 0.55$ we cannot distinguish between two regimes and we interpret this as a consequence of the practical absence of a barrier-crossing nucleation event. Whereas when $\phi = 0.54$ we observe two regimes: one characterised by pre-critical clusters ($s < s^*$) and one by post-critical clusters at large s . Therefore, in the small s regime, $-\ln(n(s)/N)$ can be interpreted as the free energy of cluster formation whose top can be read from the continuous vertical lines in Figures 6 and 7, providing an estimate for $\Delta G \sim 16$. This value is consistent with the value of the top of the free energy barrier calculated in Ref. [12, 14] for a lower packing fraction ($\phi \sim 0.535$): $\beta\Delta G^* \approx 20$. This consistency check makes us gain confidence of our cluster size distribution analysis.

Within Classical Nucleation Theory, once we know the top of the free energy barrier $\beta\Delta G^*$ and the size of the critical nucleus s^* , it is possible to estimate the difference in chemical potential between the fluid and the solid: $\beta\Delta\mu_{CNT} = \frac{2\beta\Delta G^*}{s^*}$. The value of $\Delta\mu_{CNT}$ is order-parameter dependent given that, contrary to $\beta\Delta G^*$, s^* depends on the choice of the order parameter used to identify solid-like particles [14]. Only for particular choices of the order parameter does $\Delta\mu_{CNT}$ coincide with the true value of $\Delta\mu$ (obtained, for instance, from thermodynamic integration). In our case, if we use the CNT expression for $\beta\Delta\mu_{CNT}$ taking the value of the top of the free-energy barrier and the critical nucleus size from Figure 7 ($\beta\Delta G^* = 16$ and $s^* = 50$), we obtain $\beta\Delta\mu_{CNT} = 0.64$, which is in good agreement with the value computed from thermodynamic integration $\beta\Delta\mu = 0.63$ in Ref. [14]. Thus, our choice of the order parameter to identify crystalline particles seems to be reasonable.

D. Effect on crystallization of the cutoff needed to define of a solid particle

We now study the effect of the choice of ξ_c (the parameter used to define solid-like particles in our definition of crystalline clusters), on the properties of the clusters, such as the radius of gyration. We focus on the two extreme cases studied, $\phi = 0.54$ and $\phi = 0.61$. To identify the neighbours of each particle, we use the criterion of Ref. [57] and determine the number of connections with $d_6 > 0.7$. At this point, we use various definitions of the number of connections needed for a particle to be identified as solid-like: not only $\xi_c = 6$ (what we have used so far to identify a solid-like particle), but also 8 or 10. To qualitatively understand the effect of the choice of ξ_c on the structure of the growing clusters, we represent a slab of the system taken at the same position in the sample when $\phi = 0.54$ (Figure 8 a and b) and when $\phi = 0.61$ (Figure 8 c and d). In panels a) and c) solid particles are evaluated using $\xi_c = 6$ and correspond to a system with $X \sim 0.20$ whereas in panels b) and d) they are calculated using $\xi_c = 10$ and correspond to a system with $X \sim 0.10$.

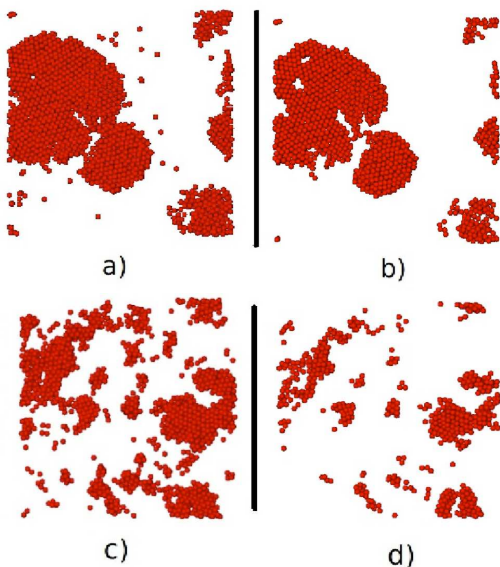


FIG. 8: Slabs (about 3-4 particles diameters thick) where solid particles are identified with: Top: $\phi = 0.54$, a) $\xi_c = 6$ ($X \sim 0.20$) and b) $\xi_c = 10$ ($X \sim 0.10$); Bottom: $\phi = 0.61$, c) $\xi_c = 6$ ($X \sim 0.20$) and d) $\xi_c = 10$ ($X \sim 0.10$).

From Figure 8, it is clear that the overall structure of the clusters is not much affected by the choice of ξ_c . Filion et al. [14] have recently evaluated the effect of the choice of ξ_c on the calculation of the top of the nucleation free-energy barrier ΔG^* at $\phi = 0.535$ (see Figure 2 in Ref. [14]), showing that ΔG^* does not depend on ξ_c (named in the same way in their work). This contrasts with the corresponding value of the size of the critical cluster s^* : for $\xi_c = 6$ they find $s^* \sim 100$, whereas for

$\xi_c = 10$ they obtain $s^* \sim 25$. The authors conclude that the main difference among the order parameters (each defined with a given value of ξ_c , $5 \leq \xi_c \leq 10$) is the ability to distinguish between fluid-like and solid-like particles near the fluid–solid interface.

To quantify our observations, we represent the radius of gyration as a function of the cluster size at packing fraction $\phi = 0.54$ and $\phi = 0.61$ (Figure 9) for different values of ξ_c .

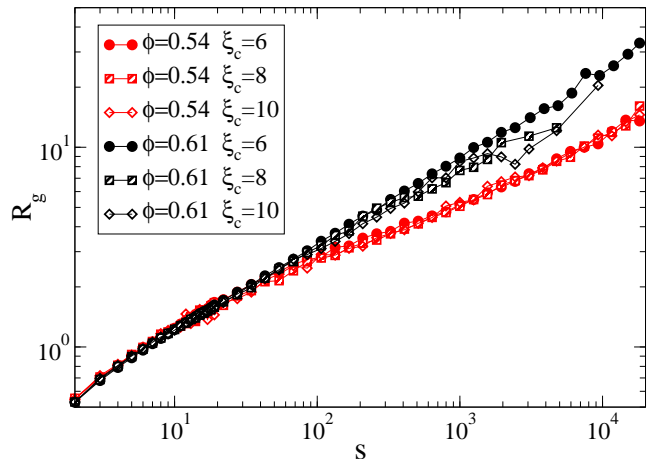


FIG. 9: R_g versus s at $\phi = 0.54$ (red) and $\phi = 0.61$ (black) averaged over time and over 10 runs. In both cases, filled circles, striped squares and empty diamonds correspond to clusters where solid-particles are defined using $\xi_c = 6$, $\xi_c = 8$, and $\xi_c = 10$, respectively. The spreading of the data for large values of s at $\phi = 0.61$ is due to poor statistics for very large clusters.

Results for $\phi = 0.54$ and $\phi = 0.61$ clearly provide evidence that R_g does not depend strongly on the different values of ξ_c used in the definition of solid-like particles. The slabs of Figure 8 corroborate the result presented in Figure 9, and we conclude that the structure of the growing crystalline clusters is not affected by the choice of ξ_c .

We now re-plot Figure 8 assigning different colours to each particle depending whether a particle has been labelled as solid-like with one of the above-mentioned criteria: in red, we colour particles that are solid-like according to the most stringent criterion ($\xi_c = 10$), in orange particles identified as solid-like using $\xi_c = 8$ (but not with $\xi_c = 10$) and in yellow particles identified as solid-like using $\xi_c = 6$ (but not with $\xi_c = 8$).

When $\phi = 0.54$ (Figure 10(left)) we observe that the criterion with $\xi_c = 10$ allows one to obtain particles in the inner part of the clusters, surrounded by particles defined as solid-like according to the looser criterion $\xi_c = 8$ and then by the ones defined with $\xi_c = 6$. During the time-evolution of the clusters, we always observe the colour-code ranging from red (black) in the inside to yellow (light grey) in the outside of the clusters. As we have already discussed, small clusters for $\phi = 0.54$ as well as branched ones for $\phi = 0.61$ are far from being compact:

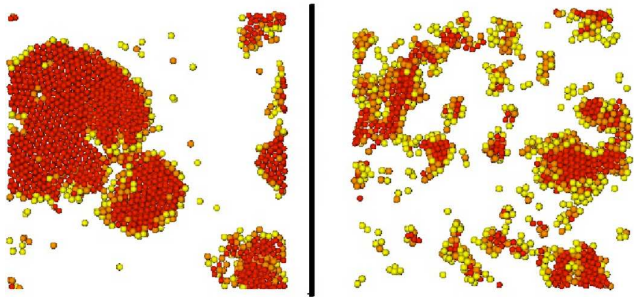


FIG. 10: Left: $\phi = 0.54$. Re-plot of Figure 8a), where we colour in red particles identified as solid-like with $\xi_c = 10$ (corresponding to the ones represented in Figure 8b), in orange particles identified as solid-like using $\xi_c = 8$ (but not with $\xi_c = 10$) and in yellow particles identified as solid-like using $\xi_c = 6$ (but not with $\xi_c = 8$). Right: $\phi = 0.61$. Re-plot of Figure 8c) with the same colour-code. Particles identified as solid-like with $\xi_c = 10$ correspond to the ones represented in Figure 8d). The colours become black, dark grey and light grey, respectively, in black-and-white.

in these cases, most particles will live at the interfaces, so that red (black) particles are less abundant.

In recent works [20–22], it has been suggested that in hard sphere systems at low packing fractions ($\phi \sim 0.54$) nucleation happens via a two-step scenario: first the formation of a locally denser regions with high bond orientational order parameter, and next the restructuring of these regions at constant density. Analogously, either at $\phi = 0.54$ and at $\phi = 0.61$, we first observe the formation of loosely packed clusters (in yellow), that become more compact when growing (in orange) and within which we identify the growth of highly ordered regions (in red). However, from our analysis one could argue that nucleation happens via a “multi-step” mechanism, and that the number of steps depends on the number of cutoffs ξ_c that are monitored, i.e. three in this case. In our previous work [33], we have demonstrated how crystallization from a glass (at $\phi = 0.61$) happens via a gradual (many-steps) mechanism, but we did not discuss the process at packing fractions below the glass transition ($\phi_g = 0.58$). As we have just shown, the mechanism of gradual growth seems to hold also in super-saturated systems just above freezing.

E. Discussion and conclusions

In this paper we have analysed the properties of clusters of solid particles during crystal growth in a system of monodisperse hard spheres. We have focused on several packing fractions beyond the fluid-crystal transition up to state points deeply in the glassy regime. Given the marked differences in the nucleation processes taking place at different ϕ , i.e. from CNT regime up to crystallization from a glass [13, 33], we expected to observe clear differences also in the properties of the growing clusters.

On the basis of the results presented here, we can clearly identify two regimes where clusters are characterised by distinct statistical properties: one pertains to $\phi \leq 0.54$ and one to $\phi \geq 0.56$. The value $\phi = 0.55$ marks the threshold between the two behaviours, showing intermediate properties.

In the low- ϕ regime ($\phi = 0.54$), CNT holds and the existence of a critical size s^* leads to a cluster size distribution which shows two distinct behaviours respectively below and above s^* (at long enough times). The structure of the clusters is loose for very small sizes ($s < 50$) and crosses to spherical and compact ($d_f = 3$) for larger sizes (this can also be visualised in the snapshots shown in Figure 1). When studying the cluster size distribution, we find analogies between crystalline clusters growing and standard clusters of attractive particles approaching percolation: the cluster size distribution seems to approach a power-law behaviour also in our case, albeit with markedly different exponents. At $\phi = 0.54$ and for $s < s^*$, the cluster distribution it is not too different from a random-percolation power-law, i.e. $f(s) \sim s^{-2.2}$. However, for $s > s^*$, $f(s)$ crosses to a clearer power-law behaviour, with a much lower effective power-law exponent, i.e. $f(s) \sim s^{-1.0}$, due to the fact that larger clusters grow in a compact way. The use of CNT has allowed us to provide estimates of the free-energy barrier at $\phi = 0.54$ and of the difference in chemical potential between solid and liquid phase that, being in agreement with thermodynamic integration calculations for the same system at the same conditions [12, 14], corroborates our choice of the order parameter used to identify solid-like particles.

In the large- ϕ regime ($\phi \geq 0.56$), the free-energy barrier to nucleation becomes negligible, so that no critical cluster size exists: small size clusters have a loose structure and do not reach a compact form when growing ($d_f \sim 2.5$). When studying the cluster size distribution, we observe a power-law behaviour for all sizes, but the exponent ($\tau \sim 1.7$) is smaller than the value predicted by random percolation ($\tau \sim 2.2$). This could be ascribed to the fact that clusters do not grow completely at random, but preferably particles become solid-like in the vicinity of solid regions, which act as seeds for further growth [33]. This mechanism should become more and more important with increasing ϕ , due to the reduced diffusion of the particles. However, the surprising result is that the same behaviour is observed for any packing fractions above $\phi = 0.56$, covering a range where the dynamics slows down by several orders of magnitude [31]. Hence, we conclude that the static properties of these clusters are not much affected by dynamics.

We also notice a striking similarity between percolation events and nucleation. When $\phi < 0.56$, clusters are more compact and take a long time to percolate: similarly, the nucleation time (defined as the time when $X = 0.20$ in Ref. [13]) is large at $\phi = 0.54$, given that crystallization is an activate process, and decreases when $\phi = 0.55$, due to the lowering of the free-energy barrier. When $\phi \geq 0.56$, clusters percolate throughout the system and the nucle-

ation time increases with ϕ due to the slowing down of particles dynamics. Of course, the resulting macroscopic crystals at all packing fractions are quite different in the two nucleation regimes, as evident from the snapshots presented in Figure 1. On the one hand, homogeneous and compact structures are found in the CNT region, where crystallization once activated proceeds to the formation of a full crystal. On the other hand, for larger ϕ , the macroscopic crystals that are formed are more heterogeneous, since they result from the branching of many sub-units. In this case, it is most likely that the final structure will have a poly-crystalline character (with different units possibly bearing a different orientation).

We stress that, for both regimes (low and high ϕ), the cluster properties are very different from those observed in a standard aggregating system, driven by attractive interactions. The main difference can be observed for small sizes, where attraction drives the growth of compact small clusters ($d_f = 3$) [41]. Then, with increasing size, the structure of the clusters remains spherical upon growth if particles are interacting via a pure attraction, while a fractal structure (decreasing d_f) is observed when additional interactions, like for example long-range electrostatic repulsion, are also at work [41, 45]. In the present case of crystalline clusters, the loose structure for the small clusters can be understood by the absence of a real attraction between the particles. Hence larger clusters become compact in the classical nucleation regime (at small supersaturations), while they turn into random fractal objects when nucleation happens without activation (at large supersaturations $\phi \geq 0.56$), so that adjacent solid particles merge and branch into a percolating cluster.

In conclusion, we have provided new insights into the growth of clusters of solid particles during the nucleation process of monodisperse hard spheres. Our results shed more light on the existence of different nucleation regimes already discussed in Ref. [13, 31–33], highlighting the influence of these onto the connective properties of the system. In particular we identify that while compact crystals are formed at small supersaturations, a crossover to the formation of fractal ramified clusters is encountered upon increasing ϕ . Surprisingly, the static properties of the growing clusters in the high- ϕ regime ($\phi \geq 0.56$) are ϕ -independent. In our previous work [33], we have demonstrated how crystallization from a glass (at $\phi = 0.61$) happens via a gradual (many-steps) mechanism, but we did not discuss the process at packing fractions below the glass transition ($\phi_g = 0.58$). In this paper we show how the mechanism of gradual growth seems to hold also in super-saturated systems just above freezing.

The two growth regimes (at $\phi < 0.56$ and $\phi \geq 0.56$) may explain the different morphology of the crystals observed at low and high ϕ in the experiments of Pusey and van Meegen [2]. However, to allow for a more detailed comparison with those experimental results, a similar investigation for slightly polydisperse hard spheres, which

should also favour fractionation and hence a stronger tendency to the formation of poly-crystals, will be the subject of a future investigation.

IV. ACKNOWLEDGEMENTS

We thank C. De Michele for the code used to generate the snapshots in Figure 1. CV and ES acknowledge financial support from an Intra-European Marie Curie Fellowship (in Edinburgh) and from a Juan de La Cierva and Ramon y Cajal Fellowship, respectively (in Madrid). WCKP, MEC and EZ acknowledge support from ITN-234810-COMPLOIDS and WCKP and MEC the EPSRC grant EP/EO30173. MEC holds a Royal Society Research Professorship. This work has made use of the resources provided by the Edinburgh Compute and Data Facility (ECDF). The ECDF is partially supported by the eDIKT initiative.

Appendix A: Local bond-order parameter

We use the rotationally invariant local bond order parameter d_6 defined as the scalar product between particle i 's q_6 complex vector and the one of each of its neighbour j , $d_6(i, j) = \sum_{m=-6}^6 q_{6,m}(i) \cdot q_{6,m}^*(j)$ (where $q_{6,m}^*$ is the complex conjugate), then averaged over all particle i 's neighbours, $N_b(i)$ [61–63]. Each component $q_{6,m}(i)$ depends on the relative orientation of particle i with respect to its $N_b(i)$ neighbouring particles, and is defined as $q_{6,m}(i) = \frac{1}{N_b(i)} \left[\sum_{j=1}^{N_b(i)} \psi_{6,m}(\theta_{i,j}, \phi_{i,j}) \right] / \left[\sum_{m=-6}^6 |q_{6,m}(i)|^2 \right]^{1/2}$ (with $m = [-6, 6]$), where $\psi_{6,m}(\theta, \phi)$ are the spherical harmonics of order 6.

In order to identify particle i 's neighbours we use the criterion of Ref. [57], that is capable of avoiding a density dependence cutoff distance r_b . We have checked that such criterion is consistent with a cutoff distance criterion, where r_b is tuned for any packing fraction. We then consider particles i and j as having a "solid connection" when their $d_6(i, j)$ exceeds the value of 0.7: particle i is then labelled as solid-like if it has at least $\xi_c=6$ solid connections.

$d_6(i, j)$ is a normalised quantity correlating the local environments of neighbouring particles, it is a real number and is defined in the range $-1 \leq d_6(i, j) \leq 1$: it decreases when thermal vibrations are present but, on average, it is close to one if particles have a solid-like environment, and around zero if particles have a fluid-like environment.

Appendix B: Values of Δs_i used to compute $f(s)$

In section III C we compute the fraction of clusters of size s , $f(s)$: each value of $f(s)$ is computed within a given

interval of width $\Delta s_i = (s_{i,max} - s_{i,min})$. In Table I we explicitly indicate all Δs_i used to calculate $f(s)$. In our calculations we have also checked that different choices of interval widths yield the same cluster size distributions, within statistical error.

TABLE I: Boundaries of the cluster size intervals, $[s_{i,max}, s_{i,min}]$, centred at s .

$[s_{i,max}, s_{i,min}]$	s	$[s_{i,max}, s_{i,min}]$	s	$[s_{i,max}, s_{i,min}]$	s
1	1	[36,45]	41	[451,600]	525
2	2	[46,55]	53	[601,1000]	800
3	3	[56,75]	65	[1001,1300]	1150
[4,7]	5	[76,95]	85	[1301,2000]	1650
[8,11]	9	[96,120]	105	[2001,3500]	2750
[12,15]	13	[121,140]	130	[3501,5000]	4650
[16,21]	17	[141,200]	170	[5001,7000]	6000
[22,25]	23	[201,250]	225	[7001,10000]	8500
[26,27]	26	[251,300]	275	[10001,15000]	12500
[28,35]	31	[301,450]	375		

- [1] B. J. Alder and T. E. Wainwright, *J. Chem. Phys.*, 1957, **27**, 1208.
- [2] P. Pusey and W. van Meegen, *Nature*, 1986, **320** 340.
- [3] P. N. Pusey, *Liquids, Freezing, and the Glass Transition*, Les Houches Session LI, J. P. Hansen, D. Levesque, and J. Zinn-Justin (Eds.), North-Holland, Amsterdam, 1991, 763-942.
- [4] W. van Meegen, V. A. Martinez and G. Bryant, *Phys.Rev.Lett.*, 2009, **102**, 168301.
- [5] V. Prasad, D. Semwogerere and E. R. Weeks, *J. Phys. : Condens. Matter*, 2007, **19**, 3102.
- [6] C. Vega and E. G. Noya, *J. Chem. Phys.*, 2007, **127**, 154113.
- [7] L. A. Fernandez, V. Martin-Mayor, B. Seoane, and P. Verrocchio, preprint *arXiv:1103.2599*, 2011.
- [8] R. P. A. Dullens, D. G. A. L. Aarts and W. K. Kegel, *Phys. Rev. Lett.*, 2006, **97**, 228301.
- [9] M. Fasolo and P. Sollich, *Phys. Rev. Lett.*, 2003, **91**, 068301.
- [10] P. Sollich and N. B. Wilding, *Phys. Rev. Lett.*, 2010, **104**, 118302; P. Sollich and N. B. Wilding, *Soft Matter*, 2011, **7**, 4472.
- [11] T. Nogawa, N. Ito and H. Watanabe, *Phys. Rev. E*, 2010, **82**, 021201.
- [12] S. Auer and D. Frenkel, *Nature*, 2001, **409**, 1020.
- [13] P. N. Pusey, E. Zaccarelli, C. Valeriani, E. Sanz, W. C. K. Poon and M. E. Cates, *Phil. Trans. Royal Soc. A.*, 2009, **367**, 4993.
- [14] L. Filion, M. Hermes, R. Ni and M. Dijkstra, *J. Chem. Phys.*, 2010, **133**, 244115.
- [15] L. Filion, R. Ni, D. Frenkel and M. Dijkstra, *J. Chem. Phys.*, 2011, **134**, 134901.
- [16] T. Schilling, S. Dorosz, H. J. Schope and G. Opletal, *J. Phys. : Condens. Matter*, 2011, **23**, 194120.
- [17] T. Kawasaki and H. Tanaka, *P. N. A. S.*, 2010, **107** 14036.
- [18] H. Tanaka, T. Kawasaki, H. Shintani and K. Watanabe, *Nat. Mater.*, 2011, **9**, 324.
- [19] T. Kawasaki and H. Tanaka, *J. Phys. : Condens. Matter*, 2011, **23**, 194121.
- [20] H. J. Schope, G. Bryant and W. van Meegen, *Phys. Rev. Lett.*, 2006, **96**, 175701.
- [21] T. Schilling, H. J. Schope, M. Oettel, G. Opletal and I. Snook, *Phys. Rev. Lett.*, 2010, **105**, 025701.
- [22] J. Russo and H. Tanaka, preprint *arXiv:1109.0107*, 2011.
- [23] W. K. Kegel, *Langmuir*, 2000, **16**, 939.
- [24] Z. Cheng, P. M. Chaikin, J. Zhu, W. B. Russel and W. V. Meyer, *Phys. Rev. Lett.*, 2002, **88**, 015501.
- [25] M. D. Rintoul and S. Torquato, *J. Chem. Phys.*, 1996, **105**, 9258.
- [26] G. Brambilla, D. El Masri, M. Pierno, L. Berthier, L. Cipelletti, G. Petekidis, A. B. Schofield, *Phys. Rev. Lett.*, 2009, **102**, 085703.
- [27] W. van Meegen and S. R. Williams, *Phys. Rev. Lett.*, 2010, **104**, 169601.
- [28] J. Reinhardt, F. Weysser and M. Fuchs, *Phys. Rev. Lett.*, 2010, **105**, 199604.
- [29] G. Perez-Angel, L. E. Sanchez-Diaz, P. E. Ramirez-Gonzalez, R. Juarez-Maldonado, A. Vizcarra-Rendon and Magdalena Medina-Noyola, *Phys. Rev. E*, 2011, **83**, 060501.
- [30] W. C. K. Poon, E. R. Weeks and C. P. Royall, *Soft Matter*, 2012, **8**, 21.
- [31] E. Zaccarelli, C. Valeriani, E. Sanz, W. C. K. Poon, M. E. Cates and P. N. Pusey, *Phys. Rev. Lett.*, 2009, **103**, 135704.
- [32] C. Valeriani, E. Sanz, E. Zaccarelli, W. C. K. Poon, M. E. Cates and P. N. Pusey, *J. Phys. : Condens. Matter*, 2011, **23**, 194117.
- [33] E. Sanz, C. Valeriani, E. Zaccarelli, W. C. K. Poon, P. N. Pusey and M. E. Cates, *Phys. Rev. Lett.*, 2011 **106**, 215701.
- [34] H. Levit, Z. Rotman and E. Eisenberg, *Phys. Rev. E*, 2012 **85**, 011502.
- [35] L. J. Peng, J. R. Morris and Y. C. Lo, *Phys. Rev. B*, 2008, **78**, 012201.
- [36] J. D. Stevenson and P. G. Wolynes, *J. Phys. Chem. A*, 2011, **115**, 3713.
- [37] D. Stauffer and A. Aharony, *Introduction to Percolation Theory*, CRC Press, 1994.
- [38] N. Sator, *Phys. Reports*, 2003, **376**, 1.

- [39] J. Groenewold and W. K. Kegel, *J. Phys. Chem. B*, 2001, **105** 11702.
- [40] F. Sciortino, S. Mossa, E. Zaccarelli and P. Tartaglia, *Phys. Rev. Lett.*, 2004, **93**, 055701.
- [41] S. Mossa, F. Sciortino, P. Tartaglia and E. Zaccarelli, *Langmuir*, 2004, **20**, 10756.
- [42] A. J. Archer and N. B. Wilding, *Phys. Rev. E*, 2007, **76**, 031501.
- [43] A. Stradner, H. Sedgwick, F. Cardinaux, W. C. K. Poon, S. U. Egelhaaf and P. Schurtenberger, *Nature*, 2004, **432**, 492.
- [44] A. I. Campbell, V. J. Anderson, J. S. van Duijneveldt and P. Bartlett, *Phys. Rev. Lett.*, 2005, **94**, 208301.
- [45] F. Sciortino, P. Tartaglia and E. Zaccarelli, *J. Phys. Chem. B*, 2005, **109**, 21942; A. I. Campbell, V. J. Anderson, J. van Duijneveldt, and P. J. Bartlett, 2005, *Phys. Rev. Lett.*, **94**, 208301.
- [46] F. Cardinaux, A. Stradner, P. Schurtenberger, F. Sciortino and E. Zaccarelli, *Euro Phys. Lett.*, 2007, **77**, 48004.
- [47] E. Zaccarelli, *J. Phys. : Condens. Matter*, 2007, **19**, 323101.
- [48] P. Charbonneau and D. R. Reichman, *Phys. Rev. E*, 2007, **75**, 050401.
- [49] J. C. F. Toledano, F. Sciortino and E. Zaccarelli, *Soft Matter*, 2009, **5**, 2390.
- [50] C. Klix, P. Royall and H. Tanaka, *Phys. Rev. Lett.*, 2010, **104**, 165702.
- [51] F. Cardinaux, E. Zaccarelli, A. Stradner, S. Bucciarelli, B. Farago, S. U. Egelhaaf, F. Sciortino and P. Schurtenberger, *J. Phys. Chem. B*, 2011, **115** 7227.
- [52] E. Sanz, C. Valeriani, D. Frenkel and M. Dijkstra, *Phys. Rev. Lett*, 2007, **99**, 055501.
- [53] K. F. Kelton, *Crystal nucleation in Liquids and Glasses*, 1991, Academic Press, 75-177, 1994.
- [54] P. G. Debenedetti, *Metastable Liquids*, Princeton University Press, 1994.
- [55] D. C. Rapaport, *The Art of Molecular Dynamics Simulation*, Cambridge University Press, 1995.
- [56] E. Zaccarelli, G. Foffi, K. A. Dawson, S. V. Buldyrev, F. Sciortino and P. Tartaglia, *Phys. Rev. E*, 2002, **66**, 41402.
- [57] J. van Meel, L. Filion, C. Valeriani and D. Frenkel, in preparation (2011).
- [58] To make sure that the average procedure does not cause any loss of information, we have also plotted R_g raw data (without any average) and compare them with the curve obtained by averaging (data not shown). We then confirm that the average does not alter the information, and no modification in the cluster-structure takes place while averaging over time and over independent runs.
- [59] We have proved that the distributions averaged over another X -interval, namely $0.2 < X < 0.6$, are identical within statistical error to the ones reported here and averaged over $0.6 < X < 0.14$. This reinforces the idea that during the growth of X a stationary cluster size distribution emerges.
- [60] C. Donati, S. C. Glotzer, P. H. Poole, W. Kob and S. J. Plimpton, *Phys. Rev. E*, 1999, **60**, 3107.
- [61] P. J. Steinhardt, D. R. Nelson and M. Ronchetti, *Phys. Rev. B*, 1983, **28**, 784.
- [62] J. S. van Duijneveldt and D. Frenkel, *J. Chem. Phys.*, 1992, **96**, 4655.
- [63] P. R. ten Wolde, M. J. Ruiz-Montero and D. Frenkel, *Faraday. Discuss.*, 1996, **104**, 93.